MACHINING SCIENCE AND TECHNOLOGY
Vol. 8, No. 2, pp. 193–210, 2004

Kinematics and Wear of Tool Blades for Scrap Tire Shredding

Albert J. Shih[1,*] and Ryan C. McCall[2]

[1]Department of Mechanical Engineering, University of Michigan, Ann Arbor, Michigan, USA
[2]Department of Mechanical and Aerospace Engineering, North Carolina State University, Raleigh, North Carolina, USA

ABSTRACT

The wear of tool blades for cost-effective scrap tire shredding is investigated. Rotary disk cutters are widely used for cutting scrap tires into small pieces. The hard, wear-resistant tool blades mounted on the periphery of disk cutters maintain a narrow gap between blades and generate the cutting action. The kinematics of the relative motion of two adjacent disk cutters is derived to model the overlap region on blades during cutting. The model predictions match well with the actual shapes of the worn regions on used tool blades. The wear of tool blades made of AISI D2 and CRU-WEAR (CW) tool steels for scrap tire shredding is evaluated. A coordinate measurement machine was used to measure the tool wear. The wear on the blade surface is not uniform. Regions with high wear rate are explained using the kinematics analysis. The CW blades show a lower wear rate, about half of that of D2 blades, and a potential choice for cost savings.

Key Words: Scrap tire processing; Kinematics; Tool wear.

*Correspondence: Albert J. Shih, 1029 HH Dow, Department of Mechanical Engineering, University of Michigan, Ann Arbor, MI 48109, USA; Fax: 1-734-936-0363; E-mail: shiha@umich.edu.

DOI: 10.1081/MST-200028728
1091-0344 (Print); 1532-2483 (Online)

www.dekker.com

INTRODUCTION

Tires are nowadays designed and manufactured to be durable, wear-resistant, and stable in harsh environments. These performance advancements of tires typically make the processing of scrap tires more difficult. Annually, over 270 million scrap tires are discarded in the United States. Scrap tires, if left unprocessed, can last for long periods of time and become environmentally hazardous. There are three major usages of scrap tires. One is the tire-derived fuel (ASTM D6700-01, 2001; Clark et al., 1993; Reisman, 1997; Snyder, 1998). Under a controlled environment, tires can be cleanly burned as an energy source. Depending on the burner design, either the whole tires or shredded tire pieces are used. The second usage of shredded scrap tire pieces is for landfill, septic drainage, and other civil engineering applications to replace heavy and more expensive aggregates (ASTM D6270-98, 1998; Clark et al., 1993; Duff, 1995; Everett et al., 1996; Snyder, 1998). The third application of scrap tires is to produce the crumb rubber, which can be used in rubber-modified asphalt for more durable road pavements or molded to make cushion and vibration isolation parts (Clark et al., 1993; Snyder, 1998).

Most of the scrap tire applications require shredding to produce small tire pieces with a uniform size. The most commonly used scrap tire shredding machines, as shown in Fig. 1, consist of arrays of rotating disk cutters driven by two parallel shafts rotating in opposite directions. Two operations, designated as the primary and secondary shredding, are commonly used to cut scrap tires into small pieces. Figs. 1(a) and 1(b) show the arrangement and spacing of the disk cutters in the primary and secondary tire shredding machines, respectively. The spacing between the disks, w, as shown in Fig. 1(a), determines the average width of pieces cut. The whole tires are processed using the primary shredder with spacing between disk cutters, w, of about 150 mm. Figure 2(a) shows a picture of a primary shredder cutting scrap tires. A tire cut by the primary shredder is shown in Fig. 2(b). After primary shredding, the pieces of scrap tire are further processed by the secondary shredder with an average spacing between disk cutters, as shown in Fig. 1(b), varying from 40 to 50 mm. The scrap tire pieces may go through the secondary shredder several times until the size meets the specification.

The concept of rotary disk cutting was first developed by Kurt Rosler in the 1960s (Snyder, 1998). It has been used extensively for scrap tire shredding applications. As shown in Fig. 3, two rotating disks shear or cut the tire. The narrow gap between a set of two disk cutters, denoted as t in Fig. 1, generates the cutting action. Figure 3(a) shows the side view of two disk cutters and the cross-section of a tire with steel wires and beads. The cross-section A-A is shown in Fig. 3(b), which illustrates two tool blades and the gap, t. Figure 3(b) also indicates the tool blade wear regions, which occur close to the gap between tool blades on the periphery of disk cutters.

The three-body wear due to sand and other hard debris carried by scrap tires has been identified as the major blade wear mechanism (Snyder, 1998). The blade wear increases the gap width, t, and gradually deteriorates the shearing or cutting action. As the gap reaches a threshold level, the steel wire in the tire starts to pull out and the rubber is drawn between blades in the cut region. This creates the high friction force between adjacent blades and increases the power required for shredding. Eventually,

Marcel Dekker, Inc.
270 Madison Avenue, New York, New York 10016

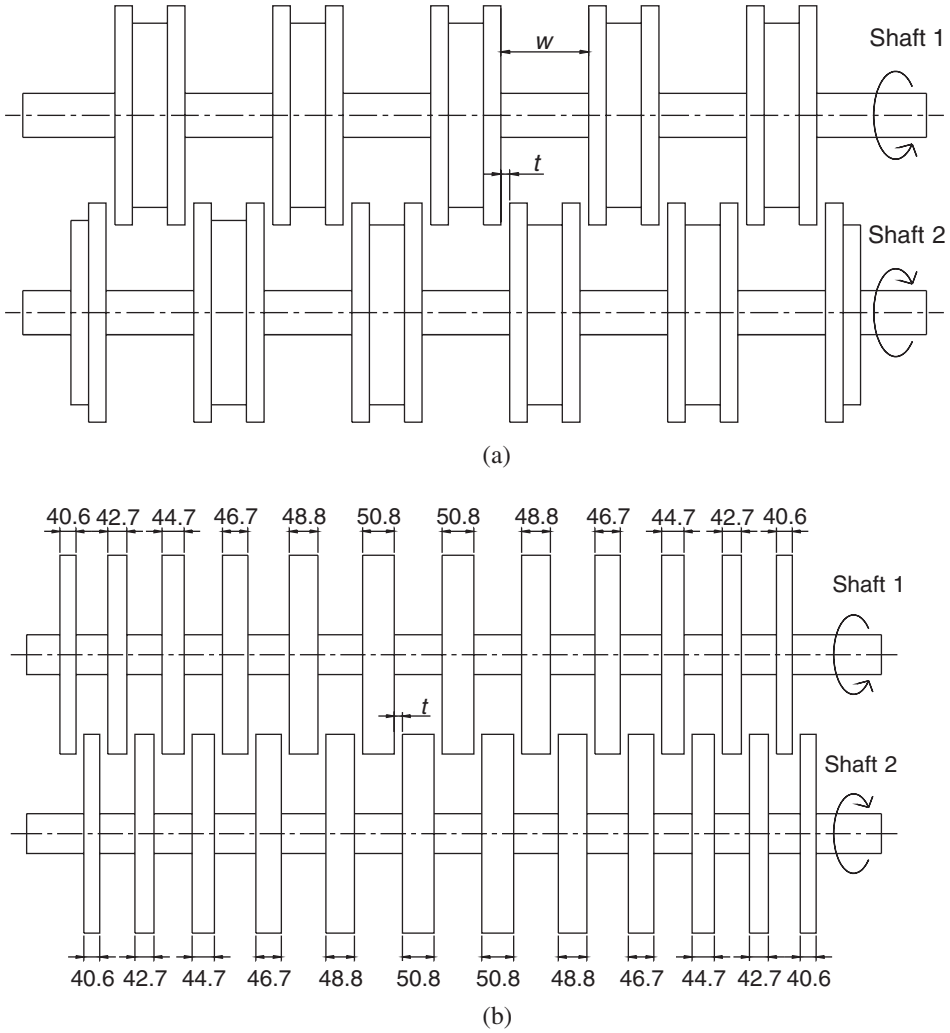

Figure 1. Configuration of rotary disk cutters used for primary and secondary shredding of scrap tires. (a) Primary shredding and (b) Secondary shredding (unit: mm).

the side surfaces on worn blades need to be reground to remove the wear region and restore the blade sharpness for reuse.

Cost is an important criterion in the development of feasible and sustainable scrap tire processing technologies. Tooling and labor costs are two major expenses in shredding scrap tires (Snyder, 1998). Each disk, as shown in Fig. 4(a), consists of 12 removable blades made of wear-resistant tool steels. The primary shredding machine shown in Fig. 1(a) has 240 blades on 20 cutting disks. The secondary shredding machine shown in Fig. 1(b) has 288 blades on 24 cutting disks. These numbers illustrate the significance of tooling cost for shredding scrap tires. Tool wear reduction is important to reduce the cost for scrap tire shredding. The labor cost to

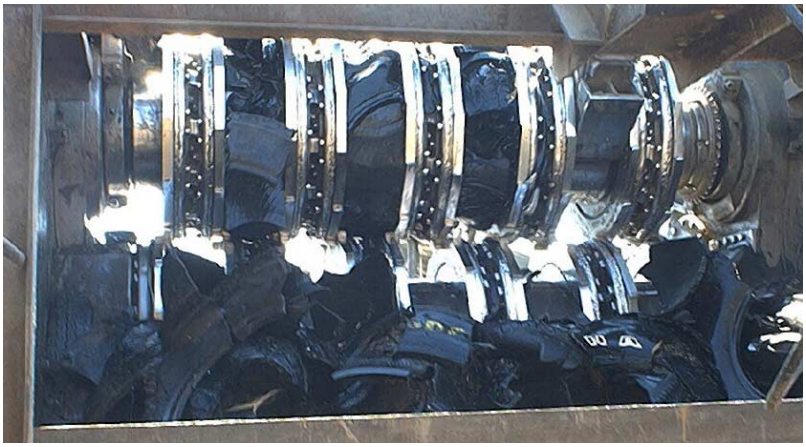

(a)

(b)

Figure 2. Photographs of the scrap tire primary shredding using rotating disk cutters and a shredded tire. (a) Primary shredding of the whole tire and (b) A tire after primary shredding. *(View this art in color at www.dekker.com.)*

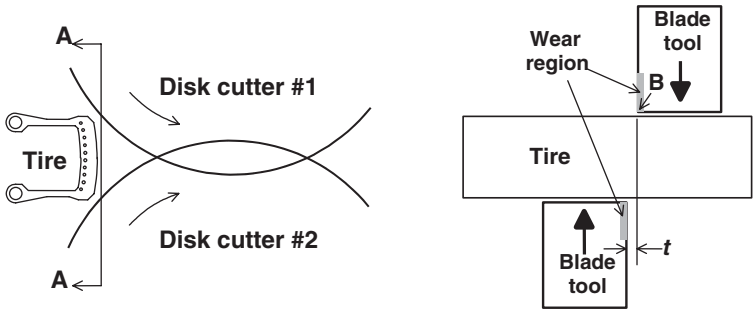

(a) (b)

Figure 3. The cutting action of scrap tires by two disk cutters and the wear region in tool blades. (a) Side view and (b) Cross-section A-A.

Marcel Dekker, Inc.
270 Madison Avenue, New York, New York 10016

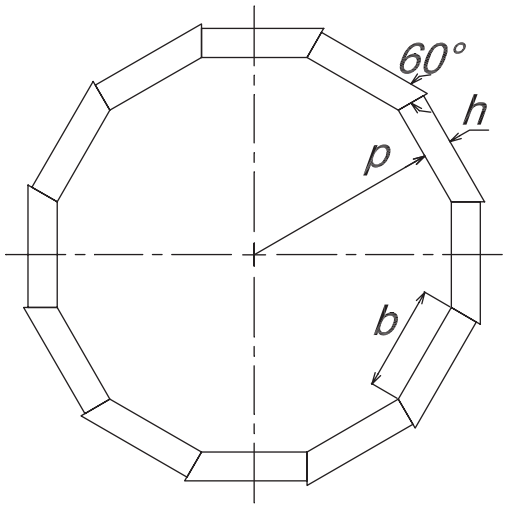

(a)

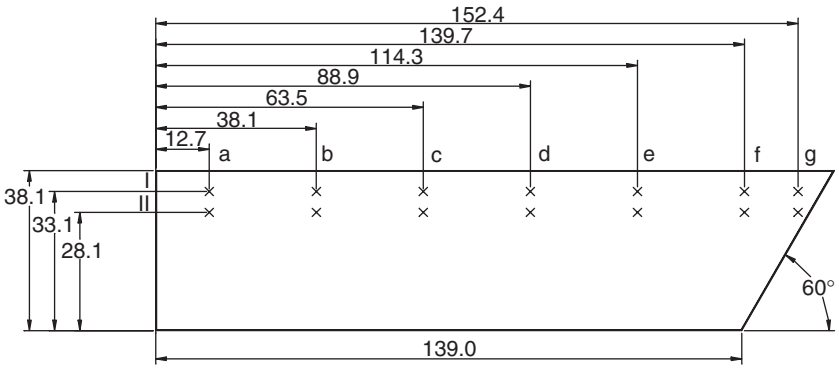

(b)

Figure 4. Arrangements and dimensions of disk cutter and blade. (a) Dodecagon-shaped tool holder and twelve blades and (b) Dimensions and wear measurement points of a blade (unit: mm).

replace and realign all worn blades on the disk cutters with a precise, narrow gap is also noteworthy in the total operation cost.

Better, more wear-resistant tool steels can be used to increase the blade life and reduce the machine down time and labor cost. Blades made of more expensive and wear-resistant tool steels can increase the tool life to a level that the overall operation cost for scrap tire shredding is reduced. Three goals of this research are to: (1) select and test a more wear-resistant material for the tool blade, (2) study the wear pattern and kinematics of disk cutting, and (3) measure the blade wear and compare the performance of two different tool steels.

In this article, the evaluation and selection of a new tool blade material are first introduced. The kinematics of the disk cutting is then derived. Modeling results are compared to experimental observations. Tool wear measurement using a coordinate measurement machine (CMM) is described. Results and discussions of tool wear are then presented.

TOOL MATERIAL SELECTION

In the past decade, two popular blade materials used for scrap tire shredding have been the AISI 4340 and D2 tool steels. AISI 4340, heated-treated to about 40 Rc, was the blade material used in early scrap tire shredding machines. The AISI D2 tool steel, denoted as D2 hereafter, can be air hardened to about 60 Rc and is more wear-resistant than AISI 4340. D2, although more expensive than AISI 4340, is one of the lowest cost tool steels and has become a popular choice of blade material for scrap tire shredding applications. The typical composition of D2 is 12% Cr, 1% Mo, 1% V, 1.5 % C, Fe accounting for the balance. D2 is a widely used tool steel and has been studied extensively. For example, Ma et al. (2000) investigated the abrasive wear of hardened D2 tool steel and Poggie and Wert (1991) studied the effect of surface finish and residual stress on the wear of D2 tool.

The design of blades with inserts made of tungsten carbide in cobalt matrix (WC-Co) was considered but was not adopted due to the following reasons. First, the blade is subject to impact forces from foreign objects hiding in scrap tires. Most of the D2 blades used in scrap tire shredding have impact chipping damages. The brittle WC-Co inserts are more likely to chip and break rapidly under the impact force. Second, a tool steel blade with WC-Co inserts needs a different grinding technology, most likely CBN grinding, to restore sharpness for reuse which would increase tooling and operating costs. Third, the design of a secure, easy to remove and install, and cost-effective way to fixture WC-Co inserts on the tool blade is not trivial. With these considerations, the WC-Co insert in tool blade was not used in this study. Therefore, this research is focused on the selection of another type of tool steel that is more wear-resistant than D2 and still cost-effective.

A wide variety of tool steels and heat treatment procedures are available for selection Roberts et al. (1998). In this study, three alternative tool materials, CRU-WEAR (denoted as CW hereafter), CPM 3V, and M-42, were evaluated. During the selection process, users of the scrap tire shredding machines imposed very strict constraints on cost. The cost of heat-treated blades made of CPM 3 V and M-series tool steels are, in general, two to four times more expensive than D2. The low toughness of the hard, wear-resistant M-series tool steel is also a concern. CW tool steel contains about 7.50% Co, 2.40% V, 1.60% Mo, 1.15% W, 1.10% C, 1.10% Si, 0.35% Mg, balanced by Fe. It can be air hardened and has a good combination of hardness, wear-resistance, toughness, and cost (Tarney, 1997; Tool Steel and Specialty Alloy Selector, 2002). The basis for improved wear resistance in CW tool steel is the substitution of higher hardness vanadium carbide (28 to 30 GPa Vickers hardness) for the chromium carbide (18 to 22 GPa Vickers hardness) in D2.

A hardness measurement in the Rockwell C scale was conducted on worn CW and D2 blades to compare their mechanical properties. The hardness indents were made in both worn and unworn regions of tool blades. An average hardness of 61.0 and 58.3 Rc in the worn region and 59.3 and 56.0 Rc in the unworn region was recorded for the heat-treated CW and D2 blades, respectively. This indicates that the CW blade is a harder and potentially more wear-resistant tool steel than the D2 blade.

In this study, twelve CW blades were mixed with 276 D2 blades in a secondary shredding machine (Fig. 1(b)) to compare the performance of these two tool materials. After shredding scrap tires for 15 days with an average operating time of 10 h per day, the worn blades were removed and examined. The next section discusses the kinematics of relative motion of a set of two disk cutters to analyze the worn region on tool blades.

KINEMATICS OF TOOL BLADE CUTTING

The arrangements and dimensions of the twelve tool blades on the dodecagon-shaped tool holder for the disk cutter used in this study are shown in Fig. 4(a). The shortest distance from the side of the polygon tool holder to its center is designated as p. The height of the blade is h. Each blade has a 60° angle tip to allow the stacking of blades around the dodecagon-shaped tool holder. Figure 4(b) shows the geometry and dimensions of the tool blade and the location of two rows and seven columns of wear measurement points used in this study. The base for the blade b is equal to $2p\tan 15^\circ$. In this study, the actual disk tool geometry of $p = 259.5$ mm, $h = 38.1$ mm, and $b = 139.0$ mm were used.

Two adjacent counter rotating disks are used as a set to shred scrap tires. Figure 5 shows the front view of the arrangement of two disks, marked as Disk 1 and Disk 2 with centers at O_1 and O_2, respectively. The distance between O_1 and O_2 is d. Two disks rotate at the same angular speed, ω, in opposite directions. An offset angle, α, is used to specify the relative orientation of these two disks. As shown in Fig. 5(a), the angle α is zero when the outside edges of the blades in two adjacent rotating disks are parallel to each other and perpendicular to line O_1O_2 at an instantaneous time in the overlap area. The offset angle α, as shown in Fig. 5(b), is defined as the angle that Disk 2 rotates in advance from the $\alpha = 0$ position in Fig. 5(a). The range of α is from 0° to 30° for the disk with twelve tool blades (Fig. 4(a)) used in this study. The change in offset angle will alter the wear pattern on the blade surface, as will be demonstrated in the following analysis.

Figure 6 shows the kinematics of the relative motion of a point P on Disk 2 relative to a blade in Disk 1. The relative position of two disks at time t is shown in Fig. 6(a). Two coordinate systems are first defined. An x-y coordinate system is centered at O_1 and fixed on Disk 1. Another u-v coordinate system is centered at O_2 and fixed on Disk 2. The x- and u-axes are both in the direction from O_1 to O_2 at time t. The position of P in the x-y coordinate at time t is represented by:

$$\{O_1P\}_t = \{O_1O_2\}_t + \{O_2P\}_t \tag{1}$$

Marcel Dekker, Inc.
270 Madison Avenue, New York, New York 10016

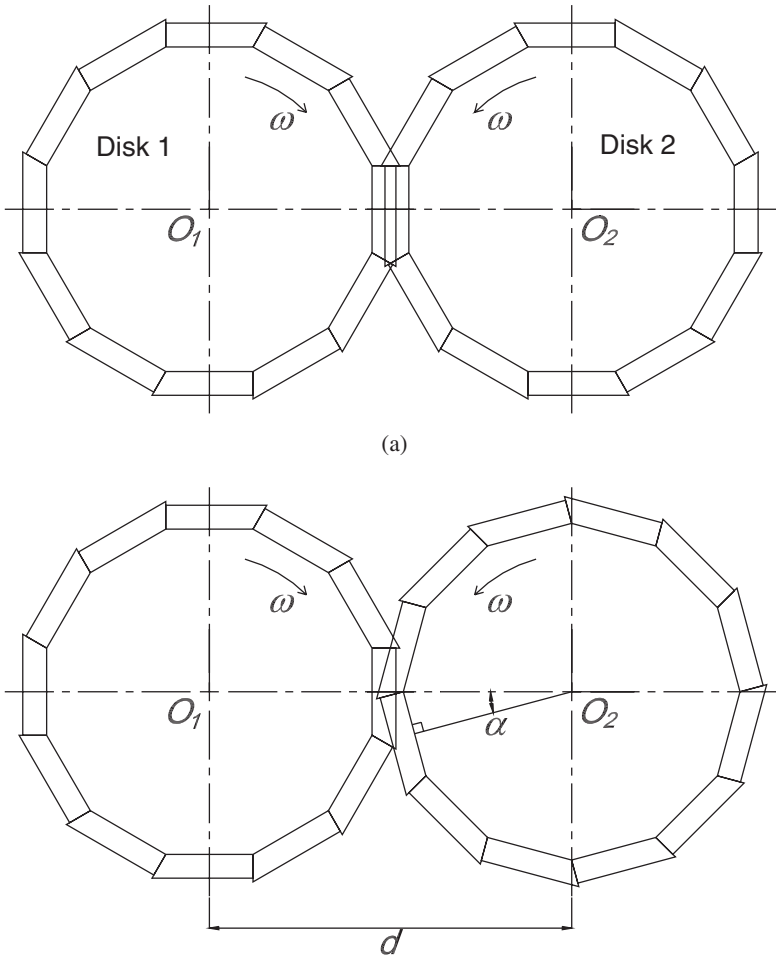

Figure 5. Definition of the offset angle α. (a) Two disks with offset angle $\alpha = 0$ and (b) Two disks offset by an angle α.

where $\{O_1P\}_t$ is the vector from point O_1 to P at time t, $\{O_1O_2\}_t$ is the vector from point O_1 to O_2 at time t, and $\{O_2P\}_t$ is the vector from point O_2 to P at time t. All vectors are referenced to the x–y coordinate system.

At time $t + \Delta t$, both disks have rotated by an angle $\theta = \omega \Delta t$ and the orientation of coordinate systems x-y and u-v has changed. As shown in Fig. 6(b), the x-y coordinate fixed on Disk 1 is rotated in the c.w. direction by an angle θ. The u-v coordinate fixed on Disk 2 is rotated in the c.c.w. direction by an angle θ. The angle between the u- and x-axes is 2θ. The point P on Disk 2 is rotated in the c.c.w. direction to the new position P'. The position of P' in the x-y coordinate at time $t + \Delta t$ is

$$\{O_1P'\}_{t+\Delta t} = \{O_1O_2\}_{t+\Delta t} + \{O_2P'\}_{t+\Delta t} \tag{2}$$

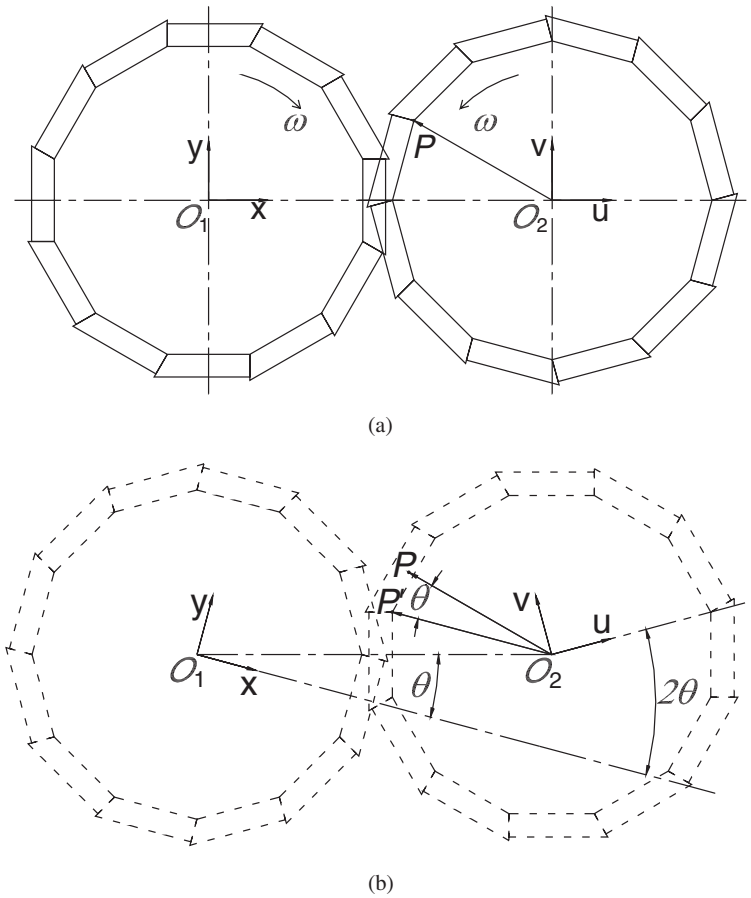

Figure 6. Analysis of the relative motion of two disk tools. (a) Time t and (b) Time $t+\Delta t$ ($\theta=\omega\Delta t$).

where $\{O_1P'\}_{t+\Delta t}$ is the vector from point O_1 to P' at time $t+\Delta t$, $\{O_1O_2\}_{t+\Delta t}$ is the vector from point O_1 to O_2 at time $t+\Delta t$, and $\{O_2P'\}_{t+\Delta t}$ is the vector from point O_2 to P' at time $t+\Delta t$. The vector $\{O_1O_2\}_{t+\Delta t}$ and $\{O_2P'\}_{t+\Delta t}$ can be derived from $\{O_1O_2\}_t$ and $\{O_2P\}_t$ using the rotational transformation matrix.

$$\{O_1O_2\}_{t+\Delta t}=[T_\theta]\{O_1O_2\}_t \tag{3}$$

$$\{O_2P'\}_{t+\Delta t}=[T_{2\theta}]\{O_2P\}_t \tag{4}$$

where

$$[T_\theta]=\begin{bmatrix}\cos\theta & -\sin\theta\\ \sin\theta & \cos\theta\end{bmatrix}$$

$$[T_{2\theta}]=\begin{bmatrix}\cos 2\theta & -\sin 2\theta\\ \sin 2\theta & \cos 2\theta\end{bmatrix}$$

Due to the rotation of both disks, the vector $\{O_2P'\}_{t+\Delta t}$ is rotated from $\{O_2P\}_t$ by an angle 2θ. This can be explained by the 2θ rotation of the u-v coordinate relative to the x-y coordinate, as shown in Fig. 6(b). Equation (2) is applied to calculate new positions of the points on the periphery of Disk 2 relative to a blade on Disk 1. Assuming the sizes of the two disks are identical, the four parameters required as the input for the analysis are: p, b, d, and α.

WEAR PATTERN MODELING RESULTS AND COMPARISON WITH EXPERIMENTAL OBSERVATION

Figure 7 shows photographs of two worn CW blades after cutting scrap tires. The modeling results of two blades on Disk 2 relative to a blade on Disk 1 at 11 different positions are also shown in Fig. 7. On one side of the blade surface, a worn region can be identified. Two distinctly different shapes of worn regions are observed in photographs of worn blades in Figs. 7(a) and 7(b). In the worn region, a pocket that penetrates deep into the blade can be seen. The wear pocket on each blade is marked in Fig. 7. Since the three parameters p (=259.5 mm), b (=38.1 mm), and d (=588.0 mm) remain the same in the scrap tire cutting test, the change in disk offset angle α is the likely cause for the different shapes of worn regions and locations of the pocket.

The distance between disk centers, d, and the offset angle, α, are difficult to measure accurately in the machine setup. These two parameters were adjusted in the modeling to match the blade overlap region to the shape of the worn regions shown in photographs of worn blades. As shown in Figs. 7(a) and 7(b), the shape of the overlap regions for $d = 588$ mm and $\alpha = 22.5^\circ$ and 7.5° exhibit good match. In Fig. 7, two blades on Disk 2 at 11 positions are marked by different line styles. Positions 1 and 11 are close to the location where the two blades on Disk 1 start and end the contact with the blade on Disk 1, respectively. The increase in each position number represents the rotation of an angle θ of 1.35° by each disk.

The overlap regions in analysis show some discrepancies to the actual shape of the worn regions in used blades. Several possible causes for such discrepancies are identified. First, the edge of the blade, as marked by B in Fig. 3(b), cannot maintain a perfect 90° sharpness. It is worn and rounded to a radius and will change the shape of the wear region. Second, the two shafts carrying heavy disk cutters will deflect slightly by the weight and cutting forces. These disks also cannot align each other perfectly as shown in Fig. 1. The deflection and misalignment create an angle of approach and departure between two disk cutters and vary the shape of the worn region. Third, all blades are assumed fixed on a perfect dodecagon-shaped tool holder. The orientation of these blades and gap between each blade can change the geometry of the ideal disk shown in Fig. 4(a) and alter the shape of the worn region.

The effect of offset angle is analyzed in Fig. 8. With the other three parameters, p, b, and d, remaining the same, the blade overlap region for six different α, starting from 0° to 25° in 5° increments, are shown in Figs. 8(a) to 8(f). At a higher offset

Marcel Dekker, Inc.
270 Madison Avenue, New York, New York 10016

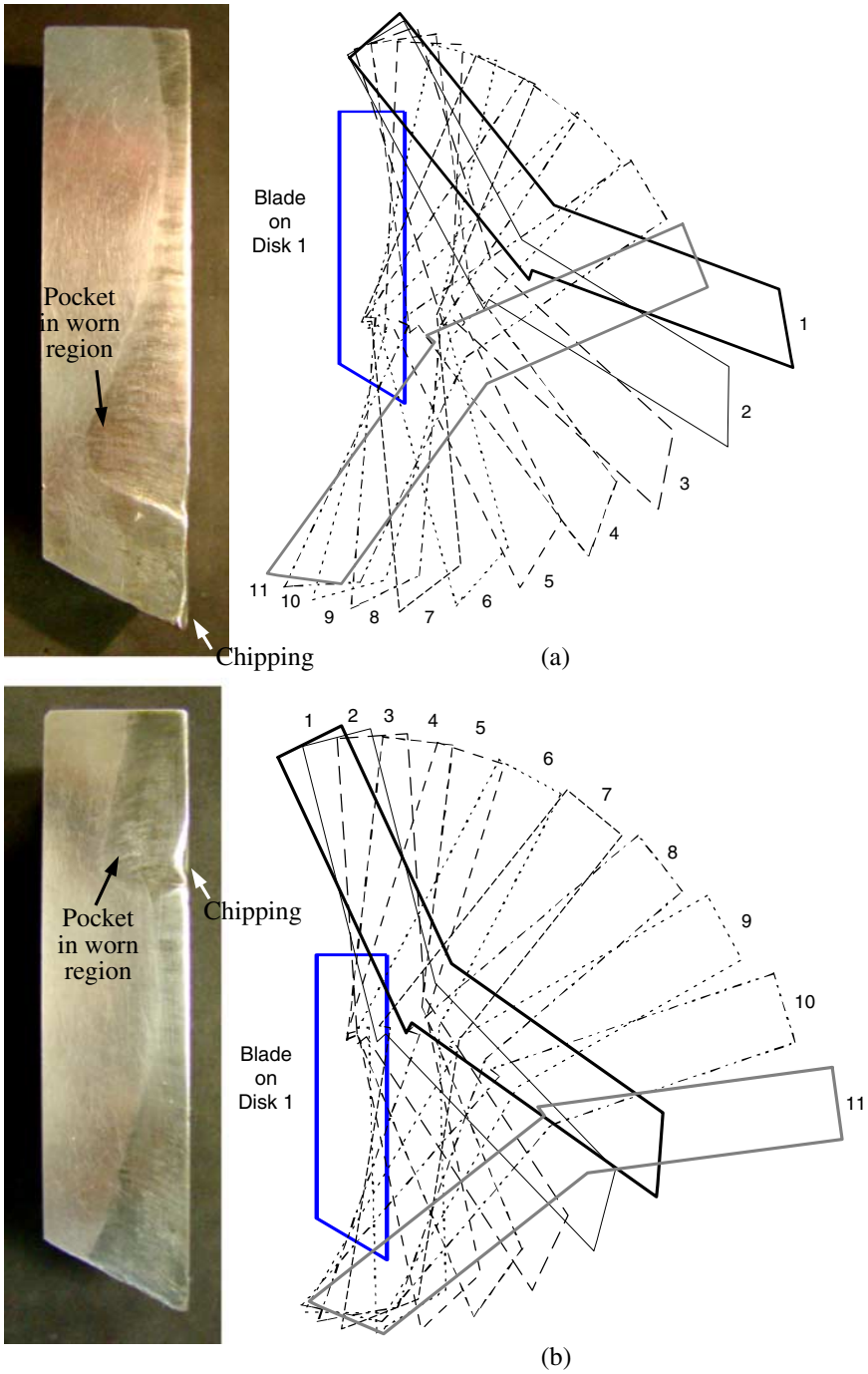

Figure 7. Photographs of the worn blades and comparison with the analysis results ($p = 259.5$ mm, $b = 38.1$ mm, and $d = 588.0$ mm). (a) $\alpha = 22.5°$ and (b) $\alpha = 7.5°$. *(View image in color online.)*

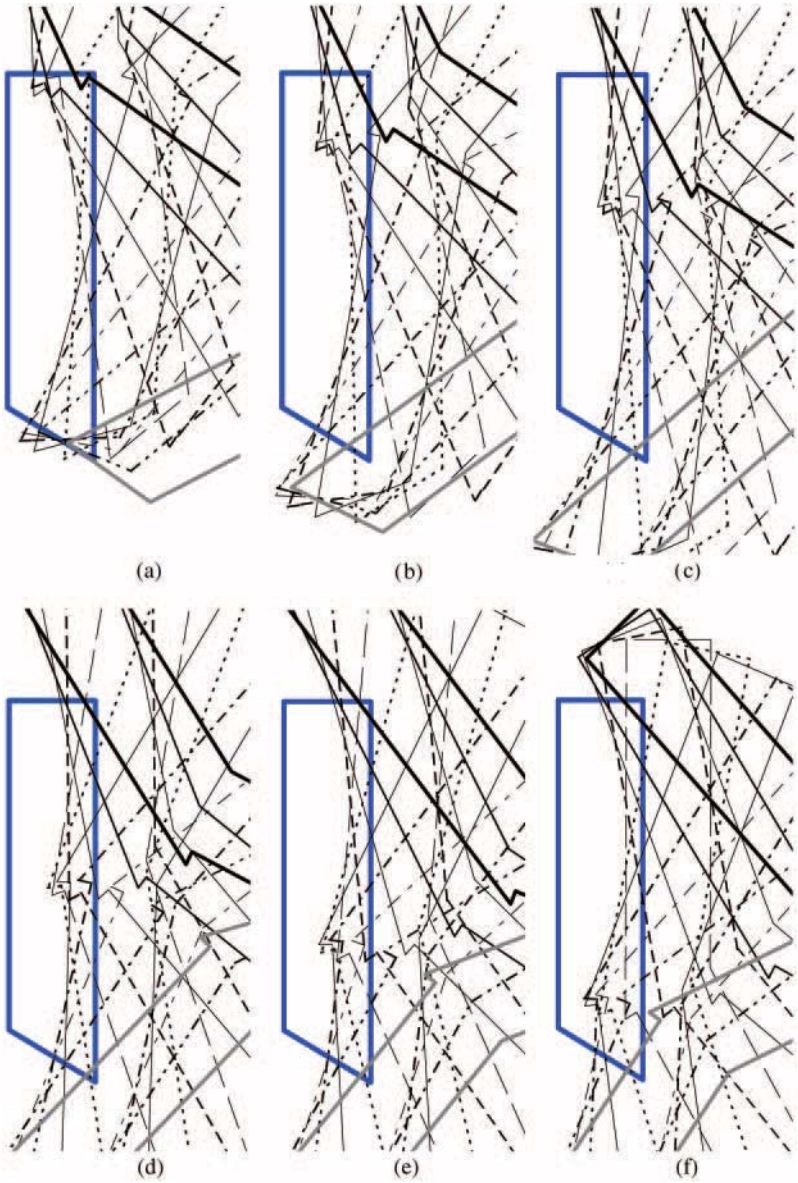

Figure 8. The effect of offset angle on the wear region ($p = 259.5$ mm, $b = 38.1$ mm, and $d = 588.0$ mm). (a) $\alpha = 0°$, (b) $\alpha = 5°$, (c) $\alpha = 10°$, (d) $\alpha = 15°$, (e) $\alpha = 20°$, and (f) $\alpha = 25°$. *(View image in color online.)*

angle, the pocket that penetrates into the blade gradually moves down from the top of the blade. This further confirms that the different worn regions observed in Figs. 7(a) and 7(b) are caused by the change in offset angle. Besides the offset angle, the center distance d can also affect the overlap area. The change in d creates

a translational movement of the blade in Disk 1 in the horizontal direction from the position shown in Fig. 8.

TOOL WEAR MEASUREMENT RESULTS AND DISCUSSIONS

A Brown & Sharpe Model Gage 2000 CMM with a Renishaw touch-trigger probe was used to measure the tool wear. The overall setup for measuring the blade wear in the CMM is shown in Fig. 9(a). Figure 9(b) shows the close-up view of the blade and the touch-trigger probe. The probe is 50 mm long with a 4 mm diameter ruby ball tip. A datum surface is first generated on the unworn region of the blade surface. The depth of wear at 14 points on the worn surface of the blade, as designated in Fig. 4(b), is recorded for blades made of CW and D2 tool steels. As shown in Fig. 4(b), two rows of measurement points are marked by rows I and II, and seven columns of points are designed from a to g.

Figures 10(a) and 10(b) show the measured wear of rows I and II of the two CW blade surfaces shown in Figs. 7(a) and 7(b), respectively. The wear is not uniform.

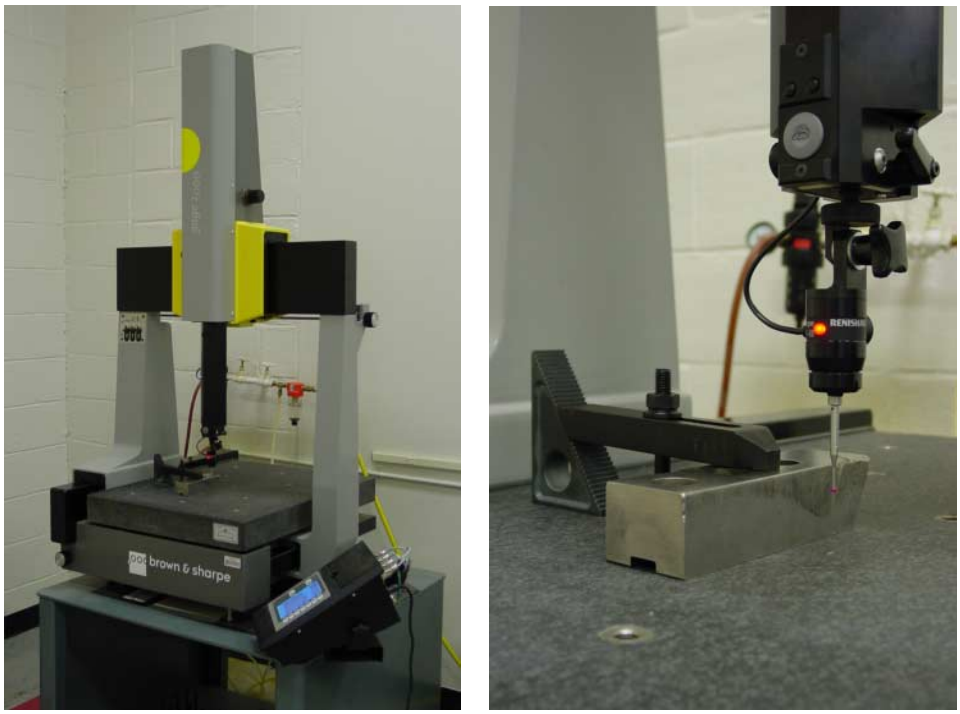

(a) (b)

Figure 9. The coordinate measurement machine and setup to measure the wear of tool blades. (a) Overview of the blade in CMM and (b) Close-up view of the blade and probe. *(View image in color online.)*

Marcel Dekker, Inc.
270 Madison Avenue, New York, New York 10016

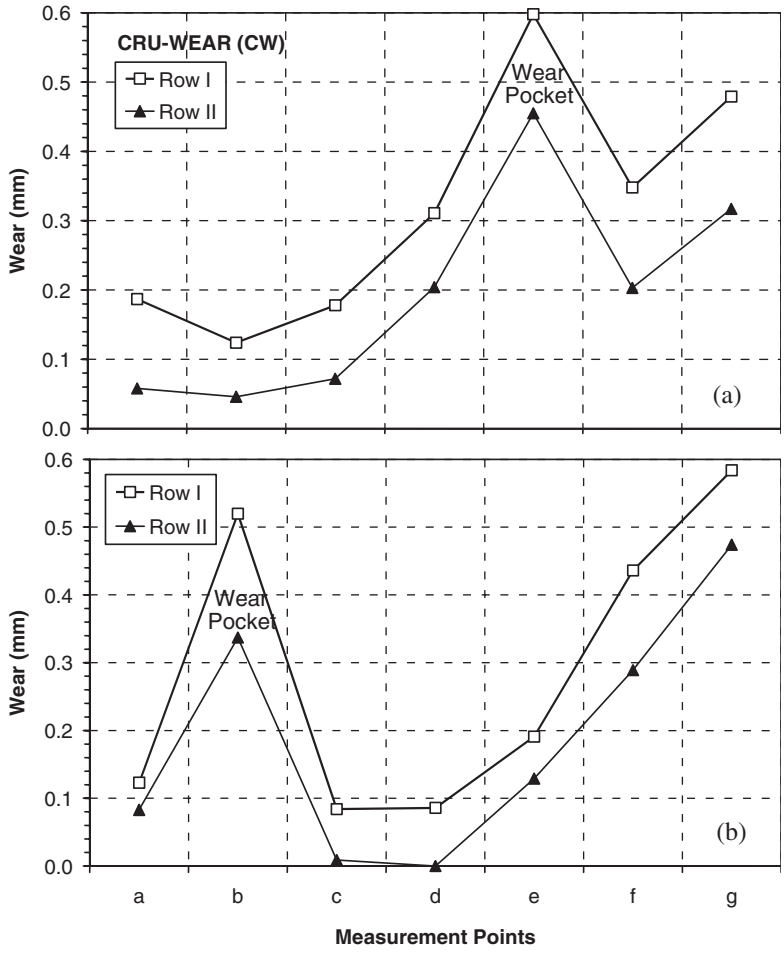

Figure 10. Wear of the CW tool blades shown in Fig. 7, (a) $\alpha = 22.5^\circ$ and (b) $\alpha = 7.5^\circ$.

A region with deeper wear occurs at point e in Fig. 10(a) and point b in Fig. 10(b). These correspond to positions of the wear pocket indicated in Figs. 7(a) and 7(b). The modeling in Fig. 7 shows the 60° tip (point g on row I in Fig. 4(b)) of the blade in Disk 2 has a transitional and slow motion in the wear pocket. This motion is likely to create the high wear in the pocket. The wear is also high at the 60° tip (point g on row I), where it rubs against the wear pocket, as shown in Figs. 7 and 8. Measurement points on row I, which are closer to the periphery of the cutter, have higher wear than that of row II. The highest level of wear measured in these two CW blades was 0.6 mm.

The wear of two D2 blade surfaces, which have been used in the same setup for the 15 day, 10 h per day scrap tire shredding test as the CW blades, is shown in Fig. 11. The most significant difference is the level of wear. The maximum wear at point g in row I is about 2 mm on both D2 blade surfaces. This

Marcel Dekker, Inc.
270 Madison Avenue, New York, New York 10016

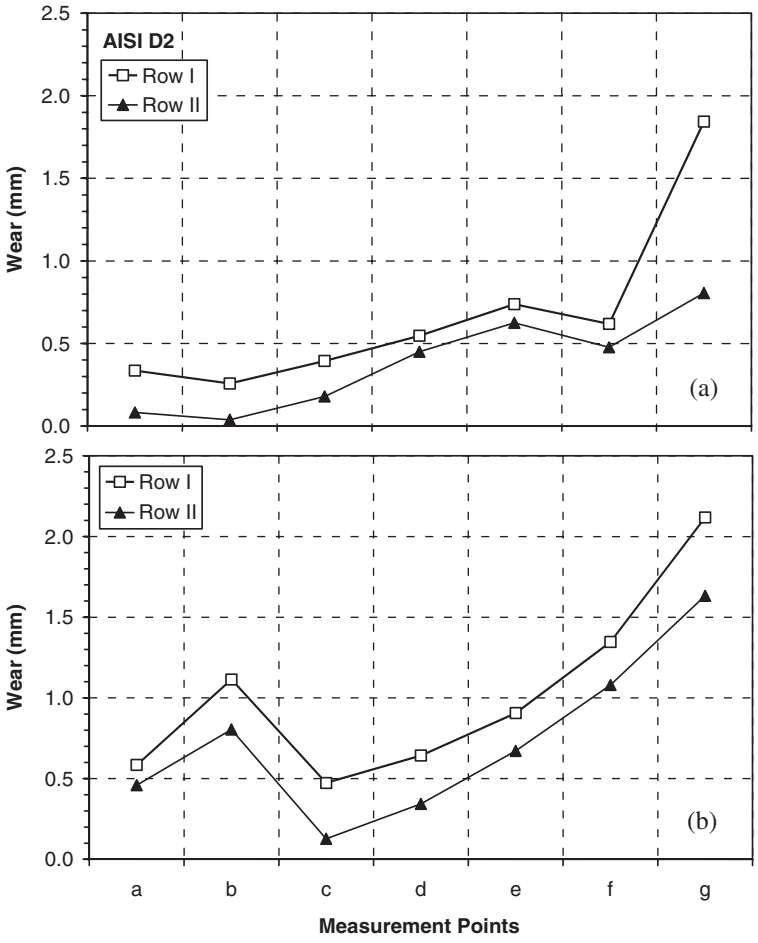

Figure 11. Wear of AISI D2 tool blades, (a) $\alpha = 22.5°$ and (b) $\alpha = 7.5°$.

illustrates the wear-resistance advantage of the CW steel for scrap tire shredding. Similar to the trend observed in Fig. 10, measurement points on row I also have higher wear than that of row II. The wear in the pocket of the worn region for the D2 blade, as shown at point b in Fig. 11(b), is not as obvious as in the CW blade.

To further quantify the wear of two tool steels used in this study, a total of twelve CW blades and eight D2 tool blades used in the test were measured using the CMM. The measured wear data of these blades were averaged and compared. Figure 12 shows the average wear of measurement points on rows I and II of the CW and D2 blades.

Chipping of the tool blade was observed on both CW and D2 blades used in this study. Examples of chipping on the blade are indicated in Figs. 7(a) and 7(b). The measurement points with chipping can be visually identified. Two graphs in Figs. 12

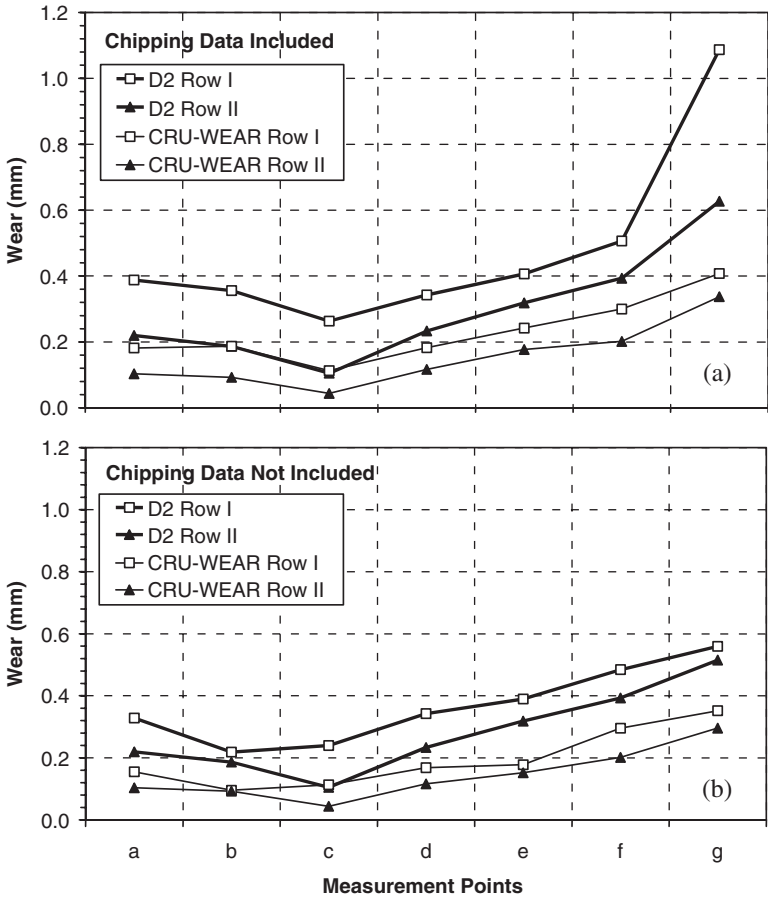

Figure 12. Comparisons of the wear of CW and D2 tool blades, (a) average tool wear with apparent chipping data included and (b) average tool wear excluding apparent chipping data.

show the average of the wear of the tool blades with and without including the points with apparent chipping. In Fig. 12(a), all the wear measurement data, including the effect from chipping, are used in the averaging and the overall wear of the tool blades is presented. Figure 12(b) shows the average wear excluding the data points with apparent chipping. Comparing Figs. 12(a) and 12(b), the wear at point g, the position prone to chipping, is reduced significantly. Figure 12 concludes that, with or without considering the effect of chipping, the CW tool blade is more wear-resistant than the D2 tool blade.

Based on Fig. 12(a), the average of the wear at the seven points in row I of the CW and D2 tool blades is 0.23 and 0.48 mm, respectively. Excluding the measurement points with chipping, the average of the wear at the seven points in row I of the CW and D2 tool blades is 0.19 and 0.37 mm, respectively. In general, the CW tool blade wears about twice slower than the D2 tool blade.

Marcel Dekker, Inc.
270 Madison Avenue, New York, New York 10016

The cost of CW tool blade is more expensive, but usually not twice more expensive than the D2. Further operational cost savings can be achieved by extending the tool changeover period and reduce the machine down time and labor cost for replacing, regrinding, and installing the tool blades.

CONCLUDING REMARKS

The wear of tool blades made of D2 and CW tool steels were evaluated for scrap tire shedding. The CW tool steel showed about half the wear rate compared to the D2. The application of tool blades made of CW tool steel potentially has an overall cost advantage. The kinematics of blades on a set of two cutter disks was derived to model the relative motion of the tool blades. The modeling of the overlap region between blades matched well with experimental observations of the wear regions on the tool blades. The analysis also showed the slow motion of the 60° tip of the tool blade around a pocket in the worn region and explained the high wear in the pocket and at the tool tip.

This research on scrap tire shredding has generated two topics worthy of further investigation. One is to understand the abrasive wear mechanism between tool blades. The kinematics modeling presented in this study is not enough to understand the blade wear. The other is the finite-element modeling of the shear cutting action to study the effect of the blade gap, t, on the scrap tire shredding.

ACKNOWLEDGMENTS

The authors acknowledge supports from the Solid Waste Division of North Carolina Department of Environment and Natural Resource, particularly the project management of Pam Moore and Paul Crissman, and the National Science Foundation (Grant #0099829). Technical assistances form Mark Diemunsch of Barclay Roto-Shred Inc., Robert Hinger of US Tire Recycling, and Edward Tarney of Crucible Materials Corp. are also gratefully acknowledged.

REFERENCES

ASTM D6270-98. (1998). Standard Practice for the Use of Scrap Tires in Civil Engineering Applications. West Conshohocken, Pennsylvania: American Society for Testing and Materials.

ASTM D6700-01. (2001). Standard Practice for Use of Scrap Tire-Derived Fuel. West Conshohocken, Pennsylvania: American Society for Testing and Materials.

Clark, C., Meardon, K., Russell, D. (1993). *Scrap Tire Technology and Markets*. Park Ridge, New Jersy: Noyes Publications.

Duff, D. P. (1995). Using tire chips as a drainage layer. *Waste Age* 26(9):6.

Everett, J. W., Gattis, J. L., Wallace, B. (1996). Drainage pipe from scrap truck tires. *Journal of Solid Waste Technology and Management* 23(1):34–43.

Ma, X., Liu, R., Li, D. Y. (2000). Abrasive wear behavior of D2 tool steel with respect to load and sliding speed under dry sand/rubber wheel abrasion condition. *Wear* 241:79–85.

Poggie, R. A., Wert, J. J. (1991). Influence of surface finish and strain hardening on near-surface residual stress and the friction and wear behavior of A2, D2 and CPM-10 V tool steels. *Wear* 149:209–220.

Reisman, J. I. (1997). *Air Emissions from Scrap Tire Combustion*, US Environmental Protection Agency Report EPA-600/R-97-115.

Roberts, G. A., Krauss, G., Kennedy, R. (1998). *Tool Steels*. 5th ed. Materials Park, Ohio: ASM International.

Snyder, R. (1998). *Scrap Tires: Disposal and Reuse*. Warrendale, Pennsylvania: Society of Automotive Engineer.

Tarney, E. (1997). Selecting high performance tool steels for metal forming tools. *Metal Forming* 31(9):35–41.

Tool Steel and Specialty Alloy Selector. (2002). Camillus, New York: Crucible Service.

Marcel Dekker, Inc.
270 Madison Avenue, New York, New York 10016